Published in final edited form as:
Dev Biol. 2013 December 15; 384(2): . doi:10.1016/j.ydbio.2013.10.005.

Cellular Mechanics of Germ Band Retraction in *Drosophila*

Holley E. Lynch[a,1], **Sarah M. Crews**[a], **Brett Rosenthal**[a], **Elliott Kim**[b], **Robert Gish**[a], **Karl Echiverri**[b], and **M. Shane Hutson**[a,b,c]

[a] Department of Physics & Astronomy, VU Station B 351807, Vanderbilt University, Nashville, TN

[b] Department of Biological Sciences, Vanderbilt University, Nashville, TN

[c] Vanderbilt Institute for Biomedical Research & Education, Vanderbilt University, Nashville, TN

Abstract

Germ band retraction involves a dramatic rearrangement of the tissues on the surface of the *Drosophila* embryo. As germ band retraction commences, one tissue, the germ band, wraps around another, the amnioserosa. Through retraction the two tissues move cohesively as the highly elongated cells of the amnioserosa contract and the germ band moves so it is only on one side of the embryo. To understand the mechanical drivers of this process, we designed a series of laser ablations that suggest a mechanical role for the amnioserosa. First, we find that during mid retraction, segments in the curve of the germ band are under anisotropic tension. The largest tensions are in the direction in which the amnioserosa contracts. Second, ablating one lateral flank of the amnioserosa reduces the observed force anisotropy and leads to retraction failures. The other intact flank of amnioserosa is insufficient to drive retraction, but can support some germ band cell elongation and is thus not a full phenocopy of *ush* mutants. Another ablation-induced failure in retraction can phenocopy *mys* mutants, and does so by targeting amnioserosa cells in the same region where the mutant fails to adhere to the germ band. We conclude that the amnioserosa must play a key, but assistive, mechanical role that aids uncurling of the germ band.

Keywords

embryogenesis; cellular mechanics; germ band retraction; amnioserosa; laser microsurgery; autonomous cell elongation

INTRODUCTION

Germ band retraction is a dynamic stage of *Drosophila* development, for which the cell and tissue movements have been well described (Campos-Ortega and Hartenstein, 1997; Schöck and Perrimon, 2002), but the cellular mechanics remain largely unknown. Two epithelia on the surface of the embryo, the germ band and the amnioserosa, move dramatically in concert. At the beginning of retraction, the germ band covers most of the dorsal and ventral surfaces of the embryo, curling around its posterior end. Other than a thin bridge over the dorsal surface, the amnioserosa is constrained to the two lateral surfaces of the embryo

Corresponding Author: shane.hutson@vanderbilt.edu, 615-343-9980.
[1]Present Address: Department of Bioengineering, Swanson School of Engineering, University of Pittsburgh, Pittsburgh, PA

(Figure 1A). As retraction proceeds, the two tissues move together as the germ band unfolds and the amnioserosa moves dorsally (Figure 1B). By the end of retraction, the amnioserosa occupies a teardrop shape on the dorsal surface of the embryo, with the surrounding germ band on the lateral and posterior surfaces (Campos-Ortega and Hartenstein, 1997; Schöck and Perrimon, 2002). During these tissue movements, individual cells change shape in a complementary fashion. Cells in the amnioserosa shorten their long axis; cells in the germ band elongate towards the amnioserosa, especially those in the closest few rows (Schöck and Perrimon, 2002). Germ band retraction is also accompanied by the formation of distinct furrows between the twelve germ band segments, T1-T3 and A1-A9, as labeled in Figure 1A,B (Campos-Ortega and Hartenstein, 1997; Hartenstein, 1993; Schöck and Perrimon, 2002).

Here, we investigate these tissue motions and accompanying cell shape changes in terms of the underlying cell- and tissue-level mechanical forces. In particular, does one tissue mechanically drive the other tissue's motion? To investigate this question, we tested two extreme alternative hypotheses. In the first, the amnioserosa plays an active and dominant mechanical role in driving the motion of both tissues, leaving the germ band to reshape passively. In the second, cell shape changes in the germ band are active and mechanically autonomous. Our results suggest that the mechanical interactions are more subtle. Many of the cell shape changes in the germ band are mechanically autonomous, but complete unfurling of the germ band clearly requires a mechanical assist from the amnioserosa.

Previous work has shown the importance of the amnioserosa for germ band retraction (Frank and Rushlow, 1996; Lamka and Lipshitz, 1999; Schöck and Perrimon, 2002; Yip et al., 1997), but its exact role has not been clear. In a set of mutations where the amnioserosa undergoes premature apoptosis (*u-shaped*, *serpent*, *hindsight*, and *tail-up*), germ band retraction fails (Frank and Rushlow, 1996). Although these phenotypes imply a role for the amnioserosa in retraction, *hindsight* mutants can be rescued to an almost wild type morphology by overexpressing a protein that is only found in the germ band (Lamka and Lipshitz, 1999). This suggests a role for the amnioserosa as a source of biochemical signals. In contrast, other research points to a more mechanical role. For example, germ band retraction fails when constitutively active or dominant negative *rhoA* constructs are expressed in the amnioserosa to disrupt its actomyosin contractility (Schöck and Perrimon, 2002). Expression of these constructs in cells along the leading edge of the germ band does not prevent retraction (Schöck and Perrimon, 2002). Furthermore, retraction fails in integrin (*scab*, *myospheroid*), laminin (*wing blister*) and laminin-regulating (*scarface*) mutants that disrupt cell-matrix interactions (Leptin et al., 1989; Schöck and Perrimon, 2003; Sorrosal et al., 2010). Integrin-mediated adhesion is required to anchor and allow active migration of amnioserosa cells over the caudal end of the germ band (Schöck and Perrimon, 2003).

Laser microsurgery has previously been used to delineate the mechanical contributions of tissues to their motions during development (Hutson et al., 2003; Kiehart et al., 2000; Peralta et al., 2007; Rauzi et al., 2008). Here we use laser microsurgery to probe the mechanical role of the amnioserosa and the germ band during retraction. The advantage of laser microsurgery is its spatial and temporal control. By investigating individual segments of the germ band, we determine that segments around the curve of the germ band behave in a way that is distinct from the rest of the tissue. Using laser microsurgery we are also able to design incisions in the amnioserosa that separate its biochemical and mechanical contributions to retraction.

MATERIALS AND METHODS

Fly strains

The primary *Drosophila melanogaster* strain used in these studies was *ubi-DE-Cad-GFP* (Oda and Tsukita, 2001) (Drosophila Genetic Research Center, Kyoto, Japan), which ubiquitously expresses E-Cadherin-GFP to label epithelial cell junctions. Where noted, we used the strain *sGMCA-3.1* (3rd chromosome insertion; gift from DP Kiehart, Kiehart et al., 2000) to label actin filaments or *Lachesin-GFP* (Edenfeld et al., 2006) to more fully label the cell surface. Cell shapes in u-shaped (*ush*) mutants (Frank and Rushlow, 1996) were analyzed by secondary antibody staining of unretracted embryos collected from a ush^2 cn^1 bw^1 sp^1/*CyO* stock (Bloomington Stock Center, Bloomington, IN).

Slide preparation and live embryo imaging

Slides of 20-30 embryos from two-hour collections were made following a modified version of previously published procedures (Ma et al., 2009). After collection, embryos were kept at approximately 15 °C until reaching germ band retraction. Some embryos were used directly after this incubation period, others were stored for a few hours at 4 °C to halt development, and later warmed during slide preparation back to room temperature. No differences were detected. Embryos were dechorionated in a 50% bleach solution, arranged on their lateral side and mounted to a cover slip using embryo glue. The embryos were left uncovered on the slide for approximately 3 minutes before being covered in halocarbon oil 27 (Sigma-Aldrich, St Louis, MO). This exposure lead to a slight dehydration that enabled flattening of the embryo, allowing more complete lateral images on a confocal system without using multiple depth slices. The embryos were finally mounted in a metal slide between the cover slip and an oxygen permeable membrane (YSI, Yellow Spring, OH). Images were captured using a Zeiss LSM410 laser-scanning confocal microscope (inverted) with a 40×, 1.3 NA oil-immersion objective. The scanning time was 8 s per frame.

Immunofluorescence microscopy of fixed embryos

For immunofluorescence of *ush* mutants, embryos from the balanced *ush/CyO* stock were collected as above, aged for a time normally equivalent to Bownes' stage 14, fixed in methanol, stained with monoclonal mouse anti-α-Spectrin (Antibody 3A9, Developmental Studies Hybridoma Bank, University of Iowa), and then with Alex Fluor 488 donkey anti-mouse IgG (Molecular Probes, Life Technologies, Grand Island, NY). These embryos are a Mendelian mix of *ush/ush*, *ush/CyO* and *CyO/CyO* – the latter viable through late embryogenesis (Hsouna et al., 2010; Means and Hays, 2007). Presumably *ush/ush* embryos are identified from confocal images as those with an unretracted phenotype and no remaining amnioserosa cells.

Laser microsurgery system

Laser microsurgery was conducted using the above confocal microscope coupled with the 3rd harmonic (355 nm) of a Q-switched Nd:YAG laser (5 ns pulsewidth, Continuum Minilite II, Santa Clara, CA). The ablating laser was targeted to specific regions of fly embryos using a computer-controlled steering mirror and a custom plug-in for ImageJ (NIH, Bethesda, MD). This plug-in allows users to draw various shapes on a recently obtained image and directs the ablating laser along the user-defined path. Extended incisions were created using multiple pulses with the physical distance between ablation sites controlled by the steering mirror's scan speed. At a 10-Hz repetition rate, achieving smooth cuts required slow scanning speeds, ~2 s for a 15-μm line.

Developmental staging via contour matching

We staged embryos' progress through germ band retraction using a contour-matching algorithm. This method augments conventional staging based on the anterioposterior position of the caudal end of the germ band (as a fraction of egg length) and can be used during post-processing of confocal images in which the ends of the embryo and the caudal end of the germ band are not visible. We use the contour of the amnioserosa-germ band boundary from the interface between segments T3/A1 to that between segments A7/A8 (Figure 1A,B). The core of the algorithm is a least squares regression to find the best alignment of two contours – allowing rotation, translation and scaling (Markovsky and Mahmoodi, 2009). We conducted exhaustive regression among contours from eight time-lapse image sequences to build a standard set of contours. Figure 1C shows representative members of this standard set; Figure 1D shows the temporal overlap between the time-lapse image sets that provided redundant coverage of the complete time course of germ band retraction. As an example, we stage an additional time-lapse image sequence, or set of "test" contours. We first perform an exhaustive least squares alignment between each contour of the "test" set and each contour of the standard set. Estimating the expected variance in aligning contours from our previous assembly of the standard set, we use a χ^2 test to construct a matrix of *p*-values representing the quality of these alignments (Figure 1E). The best-matching standard contour for each test contour is used as a measure of progression through germ band retraction (Figure 1F). We also determine a confidence interval for the staging using a variance based on the best alignment and defining the confidence interval to include all standard contours that aligned with a given test contour with $p < 0.05$. As the staging results for this test set show, the contour-staging algorithm is most reliable in mid to late germ band retraction. In early retraction, the staging is less precise because the chosen contour does not vary strongly with time. This algorithm can even be used on the fairly abnormal contours observed during laser-microsurgery experiments, with the caveat that the confidence interval can get quite wide. Contour alignments for staging were run using Mathematica (Wolfram Research, Champaign, IL).

Analysis of cell shape and alignment

Images were segmented to analyze cell shape using either Packing Analyzer (Aigouy et al., 2010) or SeedWater Segmenter (Mashburn et al., 2012). We tracked cell shape changes via both the average cellular aspect ratio and a cellular area moment of inertia tensor (Weisstein, 2013),

$$\mathbf{J}=\sum_i \begin{bmatrix} y_i^2 & -x_i y_i \\ -x_i y_i & x_i^2 \end{bmatrix} \Delta x_i \Delta y_i \quad (1)$$

where x_i and y_i are the coordinates of a single pixel (relative to the cell's centroid), Δx_i and Δy_i are the dimensions of that pixel, and the sum is taken over all image pixels *i* belonging to a single cell. This **J** tensor maintains information on cellular orientation that is lost in a simple averaging of aspect ratios. For example, the rotation that diagonalizes this tensor (to **J′**) yields the direction of one of the cell's principal axes (equivalent to the axes of its best-fit ellipse). We take α as the direction of the cell's longest principal axis and track cell elongation through the ratio of the cell's extension along its two principal axes

$$\kappa=\sqrt{\frac{\mathbf{J}'_{\max}}{\mathbf{J}'_{\min}}} \quad (2)$$

where $\mathbf{J'_{max}}$ is the largest diagonal entry in the rotated **J′** tensor and $\mathbf{J'_{min}}$ is the smallest diagonal entry. κ is equal to the aspect ratio of a cell's best-fit ellipse. The **J** tensors for

multiple cells can be averaged together and then used to calculate α and κ for a composite cell. This averaging at the tensor level maintains a dependence on the elongation direction, *e.g.*, if all the cells had individual aspect ratios of two and all were aligned in the same direction, then the composite κ would also be two, but if the cells were randomly oriented, then the composite κ would be close to one. Tracking both κ and mean aspect ratio enables a more complete description of cell shape and orientation changes. Note that the reported angles α are calculated based on the local segment coordinates. Thus, an angle has the same meaning within the segment regardless of the segment's current position in the embryo. Post-segmentation analysis of cell shapes was also conducted using Mathematica (Wolfram Research, Champaign, IL).

Image analysis

Routine analysis and image adjustments, *e.g.*, brightness/contrast and inversion, were performed in ImageJ (NIH, Bethesda, MD).

RESULTS

External forces on the germ band

If the amnioserosa plays an active mechanical role in germ band retraction, then segments of the germ band should experience an external force in the direction along which the amnioserosa contracts. Since the germ band reshapes drastically during retraction, this assessment is best done in a series of local coordinate systems, one for each germ band segment, and by allowing the local coordinate system to move with the segment. In each local coordinate system, the *y*-direction is defined to stretch from the edge of the embryo to the amnioserosa (Figure 2C-inset, red arrows), bisecting the angle between the segment's boundaries; the *x*-direction is perpendicular to that (Figure 2C-inset, blue arrows). We define the local coordinate systems so that the positive *x*-direction is in the direction of segment motion (caudal to rostral) and the positive *y*-direction is in the direction of the amnioserosa.

To determine if the germ band is subject to any external forces, we examined how the tissue reacts to small laser incisions. In each segment of the germ band, we made 15-μm line cuts along the *x* and *y* direction ($N \geq 5$ per direction per segment; only one cut per embryo) (Figure 2A, B respectively). In response to each incision, the tissue recoils from the ablation site, the wound reaches a maximum area, and then begins to heal (Figure 2C).

Since germ band retraction is a dynamic system, forces on the germ band may not be constant. We thus selected embryos to wound based on maintaining a uniform average pre-wounding stage: $\langle R \rangle = 36 \pm 30\%$ retracted when averaged over all wounding experiments. The pre-wounding stages within a set of experiments corresponding to any single segment and direction had a mean standard deviation of 29%. The mean stage varied across segments and directions with a standard deviation of 15%. Figure 3 shows the results of our comparison of these wounds at their maximum expansion. For a given segment, the wound sizes are similar in either direction. In contrast, several segments had significant direction-dependent differences in aspect ratio ($p < 0.05$ using Student's t-test with unequal variances). These segments (A4, A5, and A7) spend a large fraction of retraction in the curve of the germ band. For each, the largest aspect ratio was for incisions made in the *y*-direction – towards the amnioserosa.

These results suggest the hypothesis that anisotropic stresses in segments A4, A5 and A7 are caused by forces exerted on the germ band by the amnioserosa. To test this hypothesis, we made additional linear incisions in segment A5 and nearly simultaneously (within 10 s) ablated of one flank of the amnioserosa. These linear incisions opened up over several

minutes to mean areas and perimeters similar to those above, but their aspect ratios were different. With concurrent ablation of the amnioserosa, the mean aspect ratio ± one standard deviation for incisions along the *x*-axis of segment A5 was 1.00 ± 0.42 ($N = 6$), and that for incisions along the *y*-axis was 1.65 ± 0.52 ($N = 5$). Ablating half the amnioserosa thus leads to a fairly strong reduction in the anisotropy of wounds along the *y*-axis of segment A5, which was 2.29 ± 0.28 when the amnioserosa was intact. With this reduced anisotropy and with the larger variances observed after amnioserosa ablation, the shapes of wounds along the *x*- and *y*-directions were not significantly different. The *p*-value for this comparison is borderline ($p = 0.055$), so although these results support a model in which stress anisotropy in the germ band arises from forces generated in the amnioserosa, they do so only weakly. The complex wound healing response initiated around the ablated flank of amnioserosa prohibits this experiment from being more conclusive.

We also made similar linear incisions in the amnioserosa. Unfortunately, due to the drastically elongated shape of amnioserosa cells, it is not possible to wound several cells along the tissue's long axis with the same cut length used across the short axis. We therefore performed these incisions in sGMCA flies, a strain in which subcellular wounds can be seen in the amnioserosa (Ma et al., 2009). As for the germ band, the maximally expanded wounds for the two directions were of approximately the same size. Even though the difference between aspect ratios for the two directions was noticeable, it was not significant ($p = 0.29$) because the long-axis wounds were not sufficiently reproducible.

Role of the amnioserosa

To further test the necessity of the amnioserosa for retraction, we conducted another series of ablations in which we destroyed parts of the amnioserosa and noted the effects. Since minor incisions in the amnioserosa can heal, we quantified the progression of retraction using a contour staging method that is sensitive to even transient disruptions of retraction.

We start with a series of line incisions that destroyed the amnioserosa on one lateral side of the embryo (Figure 4A). Although this leaves the other half of the amnioserosa intact, it is sufficient to halt germ band retraction (Figure 4A′-A″). We conducted additional experiments to visually confirm that the amnioserosa is still intact on the other side. Thus, ablation of half the amnioserosa is sufficient to yield a failure of germ band retraction; however, the detailed morphology of this ablation-induced failure differs subtly from that observed in mutants of the u-shaped group (*ush*, *hindsight* and *serpent*) in which the entire amnioserosa undergoes premature apoptosis (Frank and Rushlow, 1996; Yip et al., 1997). This difference lies primarily in the ablation-induced twisting of the unretracted germ band (see Discussion).

We then conducted a series of less destructive ablations to determine the relative importance of various sections of the amnioserosa – for example, sections close to and far removed from contact with the curve of the germ band (Figure 4B, C). Two-line ablations of both regions cause incomplete retraction; however, the defects are much less severe (Figure 4B″, C″) than the failure caused by destruction of half the amnioserosa. Interestingly, the largest difference between these two cut designs is the shape of the germ band after retraction should have completed. Cuts made in the posterior curve of the germ band result in a narrower bend than those made closer to the anteriodorsal surface (Figure 4B′, C′).

To test whether this effect is mechanical and not due to an interruption of biochemical signaling between the amnioserosa and germ band, we cut along the center of the amnioserosa's long axis, destroying its mechanical integrity, while leaving cells directly adjacent to the germ band intact (Figure 4D). These wounds all caused at least a transient disruption, typically stalling retraction for about thirty minutes (Figure 4D″). Most of these

wounds heal; after wound healing begins, germ band retraction tends to resume. The one embryo that did not heal was also the one that never resumed retraction (Figure 4D′, and the blue line in Figure 4D″).

As a last test to distinguish between a biochemical and mechanical role for the amnioserosa, we consider what happens when short-range signaling is disrupted, but the mechanical integrity of the tissue is left intact. To this end, we ablated along the border between the amnioserosa and germ band (Figure 4E-G). These incisions are fairly small and heal quickly. None even transiently disrupted retraction (Figure 4E″-G″).

Germ band changes in the absence of retraction

Since ablation of the amnioserosa disrupts overall retraction, we then proceeded to investigate its impact on cell shape changes in the germ band. Despite an absence of retraction due to the loss of one lateral side of the amnioserosa (Figure 4A), furrow formation and some cell shape changes still occur (Figure 4A′, Figure 5).

At the start of retraction, cells in the curve of the germ band and along its ventrolateral aspect are only slightly elongated: <aspect ratio> = 1.57 ± 0.06 and <κ> = 1.15 ± 0.11 at a staging of <*R*> = 6 ± 19% retraction (*N* = 2 segments in each of 5 embryos with 20-50 cells per segment). The mean composite κ is lower than the mean aspect ratio because the cells are only weakly aligned. By the end of germ band retraction (<*R*> = 90 ± 12%), the cells become more elongated and more strongly aligned: <aspect ratio> = 1.72 ± 0.18 and <κ> = 1.39 ± 0.12. This trend is also evident in the rose diagrams of the control group in Figure 5. In later stages of retraction, more cells are oriented with their long axis towards the amnioserosa (more darkly shaded sectors near 90°) and these cells have longer aspect ratios (increased length of these sectors).

Although cells in control embryos elongate and align similarly in segments A2 and A5, these segments behave very differently when the amnioserosa is ablated. After ablation of one flank of the amnioserosa, elongation and alignment in segment A2 is nearly eliminated. The mean aspect ratio and mean composite κ themselves give no indication of elongation (<aspect ratio> = 1.47 ± 0.02 and <κ> = 1.16 ± 0.11 for κ = 5 embryos with <*R*> = 92 ± 9%), and the corresponding rose diagram in Figure 5 has sectors near 90° that are only slightly longer and darker. Looking at the individual experiments (Supplemental Figure S1), post-ablation alignment of cells in segment A2 was only evident in two of five embryos.

On the other hand, despite ablation of the amnioserosa, cells in segment A5 elongate and align normally: <aspect ratio> = 1.76 ± 0.05 and <κ> = 1.45 ± 0.08 for *N* = 5 embryos with <*R*> = 87 ± 14%. This indicates that cell elongation occurs normally for a segment along the germ band's curve, even without a complete amnioserosa, and even in the absence of retraction. The late stage rose diagrams for segment A5 in control and ablated embryos differ only by a slight shift in the alignment direction (last column of Figure 5), but inspection of the individual experiments shows that this shift is primarily due to a very large alignment shift in just one of five embryos (Supplemental Figure S1).

These results provide an interesting contrast with those in previous sections. During mid-retraction, segments in the curve of the germ band have high stress anisotropy – with large tensile stresses in the direction of the amnioserosa – but ablation of the amnioserosa has almost no effect on these cells' elongation and alignment. In a nearly opposite fashion, segments along the ventrolateral aspect of the germ band display low stress anisotropy, but their elongation is highly dependent on having an intact amnioserosa. These results are at odds with a simple model in which tension from the amnioserosa helps elongate and align

germ band cells, and ablation of the amnioserosa simply removes this normally assistive tension.

One obvious complication of these ablation experiments is their limitation to removing just half the amnioserosa. For comparison, we imaged *ush* mutant embryos with an unretracted phenotype in which the amnioserosa dies prematurely. Using a balanced *ush/CyO* stock, the Mendelian mix of embryonic genotypes allowed use of presumably wild-type and heterozygous embryos to gauge the collection's approximate developmental stage. By waiting long enough for most embryos to progress into mid dorsal closure (stage 14), there was a clearly identifiable minority of embryos that remained unretracted. Confocal images of unretracted embryos that were fixed and stained with anti-α-Spectrin antibodies showed a complete absence of amnioserosa cells and almost no elongation or alignment of germ band cells (Figure 5C-E). Cells in segment A5 did not elongate beyond what was normally observed in early germ band retraction (<aspect ratio> = 1.50 ± 0.05 and <κ> = 1.11 ± 0.08 for $N = 5$ embryos) and those in segment A2 barely elongated (<aspect ratio> = 1.59 ± 0.12 and <κ> = 1.29 ± 0.16 for $N = 5$ embryos). These results are clearly different from what we observed after ablation of the amnioserosa – most notably in segment A5. The implications of these differences are discussed in detail in the Discussion.

Behavior of isolated germ band cell patches

To further investigate the mechanical autonomy of cell shape changes in the germ band, we used laser microsurgery to isolate small patches of germ band ($N = 21$ patches with 9 to 63 cells each). This isolation was only with regard to apical connections. Imaging of Lachesin-GFP flies clearly showed that these patches remained attached to a more basal layer. After such apical isolation, some cells in a patch would expand while others contracted. Within 10 minutes, these cell shape changes lead on average to a ~ 20% reduction in mean cell area, but no change in mean cellular aspect ratio. Within 20 minutes, isolated cell patches either faded away completely (9 of 21) or reattached (12 of 21). That time span is too short and the normal rate of cell elongation in the germ band is too slow to conclusively determine whether mechanically isolated germ band cells continue to elongate. The limited conclusion one can draw is that external forces from tissue-wide tensile stress are not required to maintain cell elongation.

DISCUSSION

The expansion of line incisions in the germ band indicates that all segments are under tension. The local anisotropy in this tension is revealed by the differential response of wounds made parallel to the local *x*- or *y*-axis. As shown in Figure 3, all of the wounds lost their initial high aspect ratio as they expanded, but wounds in segments A4, A5 and A7 maintained a higher aspect ratio when the incision was parallel to the local *y*-axis. This suggests that the local stress in those segments is greatest in the *y*-direction, *i.e.*, towards the amnioserosa. During mid-retraction, $\langle R \rangle = 36 \pm 30\%$, this anisotropy is most evident for segments in the curve of the germ band; however, due to the dynamic nature of germ band retraction, these observations of stress anisotropy have a limited domain of applicability. They should only be considered a snapshot of the mechanical stress field. Stress anisotropy may be absent in these segments or present in other segments in earlier or later stages. Certainly, shape anisotropy in the amnioserosa is even stronger and more widespread in earlier stages, but by mid-retraction, it is limited to the amnioserosa's most posterior regions. Nonetheless, these results are clearly consistent with the amnioserosa assisting mid-retraction movements by pulling on the crook of the germ band. Such a role was previously suggested based on the convexity of the amnioserosa-germ band interface (Schöck and Perrimon, 2002). The only segment from the curve that is missing from the list above is A6,

which also had a higher aspect ratio for wounds parallel to the local *y*-axis. Variability was extremely high in this segment and the aspect ratio difference was not statistically significant.

If the amnioserosa is pulling on segments in the crook of the germ band, then cuts made along the amnioserosa's long axis should also have a higher aspect ratio than cuts made along its short axis. Unfortunately, just as for segment A6, we do observe a higher aspect ratio for the appropriate cuts, but variability is too high for this difference to be statistically significant.

Further support for a mechanical role for the amnioserosa comes from our series of destructive ablations within the amnioserosa (Figure 4A-D″). These results are consistent with the hypothesis that the amnioserosa pulls on segments in the curve of the germ band to provide a mechanical assist for the germ band's uncurling; however, these results should not be construed to imply an exclusively mechanical role. No matter how carefully done, laser ablation is a crude tool in the sense that it removes both mechanical and biochemical contributions of the ablated cells. The results here only show that the amnioserosa has an important mechanical role in addition to any role as a source of inductive signals.

In the different ablation protocols shown in Figure 4, ablation of more amnioserosa cells generally results in more severe retraction defects. Part of this trend is attributable to the embryo's inability to heal some large wounds. The wounds of Figure 4D-D′ offer an instructive example in which embryos that eventually fail to retract are those that fail to close the ablation-induced wound. Nonetheless, this same example provides evidence for the amnioserosa's mechanical role. Ablation of a linear incision along the amnioserosa midline delayed retraction in all disrupted embryos, but only until the wound healed. This could be caused by two classes of mechanisms: (1) wound healing restores the amnioserosa's mechanical integrity and ability to generate contractile forces; or (2) amnioserosa cells around unhealed wounds fail to secrete their normal biochemical signals or secrete novel signals that suppress cell shape changes in the germ band. The latter is a possibility, but the former is a near certainty. Thus, the transient disruption of retraction – even when cells adjacent to the germ band are undisturbed – suggests that the amnioserosa's role is not limited to paracrine or juxtacrine signaling; the amnioserosa's mechanical integrity is crucial. Corollary experiments specifically ablated amnioserosa cells that were directly in contact with the germ band (Figure 4E-G″), but these ablations had no discernable effect on retraction. These experiments only show that any signals secreted by the amnioserosa must be longer range than one to two cells.

Other experiments show that amnioserosal forces are not the sole driver of germ band retraction, but are instead assistive – at least under normal mechanical conditions. First, segmental furrows form in the germ band regardless of whether the amnioserosa is intact or not. Second, patch isolation experiments show that elongated germ band cells remain elongated even after isolation from amnioserosa-generated tension. A third observation – that some germ band cells elongate normally even after ablation of one flank of the amnioserosa (Figure 5B) – could also be interpreted as a germ band autonomous contribution; however, these cells do not elongate normally in *ush* mutants in which the entire amnioserosa dies prematurely (Figure 5E). Alternative interpretations of these conflicting results are discussed below.

Comparison of ablation- and mutation-induced failures in germ band retraction

Disruption of the amnioserosa via laser ablation certainly disrupts its mechanical and biochemical contributions to development, but laser ablation also drives secondary effects – most notably a wound healing response – that could alter the pattern of stress fields and the

activation of biochemical signaling pathways in surrounding tissues. Such secondary effects are unavoidable, but can hopefully be identified by careful comparison of primary disruptions with different secondary effects, *e.g.*, ablation versus mutation.

The principal relevant comparison is between *ush* mutants in which the entire amnioserosa dies prematurely and large-scale laser ablation of one lateral flank of the amnioserosa. Both certainly and reliably cause failure in germ band retraction (Figure 4A-A″ and 5C), but the unretracted morphologies differ. First, ablation of one lateral flank of the amnioserosa causes the embryo to twist. This is especially evident for cells in the crook of the germ band, some of which move around the posterior end of the embryo towards the other flank of intact amnioserosa. In *ush* mutants, such twisting is seen, but only occasionally. We do not have live imaging of *ush* mutants to see whether this occasional twisting occurs when there is asymmetric cell death in the two flanks of amnioserosa, but that is certainly what one would expect. Second, ablation of half the amnioserosa suppresses elongation of ventrolateral germ band cells (Figure 5A, segment A2), but allows near normal elongation for those in the crook of the germ band (Figure 5B, segment A5). Oddly, cells normally subjected to the largest pulling forces from the amnioserosa (A5) are the ones that actually elongate most after ablation of half the amnioserosa. In contrast, the unretracted phenotype of *ush* mutants is associated with a near complete loss of elongation for cells in both segments A2 and A5 (Figure 5D-E). In fact, the little remaining elongation is stronger in A2 than in A5, opposite what is observed after ablation.

We suggest that the apparent contradiction is traceable to an oversimplification of the tissue mechanics after ablation of just half the amnioserosa. Because the other lateral flank of amnioserosa remains intact, such ablations do not simply remove amnioserosa tension, but instead strongly disturb the normal pattern of tensile stress. The new pattern would lead to twisting of the germ band, continued anisotropic tension in segments A4-A7 (strongest in the local *y*-direction), and increased tension along the *x*-direction of ventrolateral segments T1-A3. Cells in segment A5 would still be subjected to a stress anisotropy in the *y*-direction and thus extend and align normally. Cells in segment A2 would now be subjected to an aberrant stress in the local *x*-direction that suppresses their normal *y*-directed elongation. This hypothesis could be tested in the future by computational modeling, video force microscopy or long-term double-ablation experiments in which anisotropy is probed in more than just segment A5 long after removal of half the amnioserosa. Even without such tests, it is clear that ablation of just half the amnioserosa poorly recapitulates *ush* mutants. Both convey important information about the role of amnioserosa cells in germ band retraction, but they are not equivalent. We have attempted laser ablation of both flanks of amnioserosa, but have thus far been unsuccessful.

A second and more favorable comparison is between the βPS integrin mutant myospheroid (*mys*) and ablations that disrupt anteriodorsal regions of the amnioserosa (Figure 4C-C′). Such ablations lead to incomplete retraction. Although some amnioserosa cells remain attached to the posterior crook of the germ band, there is a large dorsal gap with no amnioserosa cells. This closely resembles the morphology of *mys* embryos (Schöck and Perrimon, 2003) in which loss of integrin function prevents amnioserosa cells from attaching to and crawling over the caudal end of the germ band. Without this anchor, contraction of the amnioserosa pulls its cells near the end of the germ band down into the embryo interior. In the matching ablation protocol, the targeted region is quite close to the caudal end of the germ band and could easily disrupt connections in that region that normally anchor the amnioserosa. The ablation protocol of Figure 4B-B′, which removes a similar sized region of amnioserosa, also yields incomplete retraction, but its morphology is quite different. The much narrower gap of missing amnioserosa cells is now in the crook of the germ band. Thus, the morphology of *mys* mutants is closely and specifically matched by embryos in

which anteriodorsal regions of the amnioserosa are ablated. This is strong supporting evidence that adhesion between the caudal end of the germ band and overlying amnioserosa cells plays a key role in the mechanics of germ band retraction.

CONCLUSIONS

Our observations suggest an interesting model for germ band retraction, one in which both tissues play a role. Successful germ band retraction clearly requires mechanical integrity of the amnioserosa. This requirement does not exclude additional juxtacrine and/or paracrine signaling roles, but the amnioserosa generates critically important forces. Nonetheless, these forces do not directly assist cell shape changes in all segments of the germ band. In some, particularly those in ventrolateral regions, the mechanical role of the amnioserosa is more permissive – its intact presence prevents aberrant patterns of mechanical stress that can prevent normal cell elongation. Together these results lend credence to a model where some of the germ band changes are mechanically autonomous, but where the amnioserosa is anchored to the caudal end of the germ band, contracts dorsoventrally, and thus assists uncurling of the germ band by specifically pulling on segments around its posterior curve. Segments of the germ band in this region behave differently from those in its more ventral or dorsal sections. They are mechanically distinct, but more work is needed to explore these segmental differences.

Supplementary Material

Refer to Web version on PubMed Central for supplementary material.

Acknowledgments

This work supported by the National Science Foundation (IOB-0545679) and the National Institutes of Health (1R01-GM099107).

REFERENCES CITED

Aigouy B, Farhadifar R, Staple DB, Sagner A, Röper JC, Jülicher F, Eaton S. Cell flow reorients the axis of planar polarity in the wing epithelium of *Drosophila*. Cell. 2010; 142:773–786. [PubMed: 20813263]

Campos-Ortega, JA.; Hartenstein, V. 2nd. Springer-Verlag; Berlin: 1997. The Embryonic Development of *Drosophila melanogaster*.

Edenfeld G, Volohonksy G, Krukkert K, Naffin E, Lammel U, Grimm A, Engelen D, Reuveny A, Volk T,C,K. The Splicing Factor Crooked Neck Associates with the RNA-Binding Protein HOW to Control Glial Cell Maturation in *Drosophila*. Neuron. 2006; 52:969–980. [PubMed: 17178401]

Frank LH, Rushlow C. A group of genes required for maintenance of the amnioserosa tissue in Drosophila. Development. 1996; 122:1343–1352. [PubMed: 8625823]

Hartenstein, V. Atlas of Drosophila Development. Cold Spring Harbor Press; Long Island, NY: 1993.

Hsouna A, Nallamothu G, Kose N, Guinea M, Dammai V, Hsu T. *Drosophila* von Hippel-Lindau Tumor Suppressor Gene Function in Epithelial Tubule Morphogenesis. Mol. Cell. Biol. 2010; 30:3779–3794. [PubMed: 20516215]

Hutson MS, Tokutake Y, Chang MS, Bloor JW, Venakides S, Kiehart DP, Edwards GS. Forces for morphogenesis investigated with laser microsurgery and quantitative modeling. Science. 2003; 300:145–149. [PubMed: 12574496]

Kiehart DP, Galbraith CG, Edwards KA, Rickoll WL, Montague RA. Multiple forces contribute to cell sheet morphogenesis for dorsal closure in *Drosophila*. J. Cell Biol. 2000; 149:471–490. [PubMed: 10769037]

Lamka ML, Lipshitz HD. Role of the amnioserosa in germ band retraction of the Drosophila melanogaster embryo. Dev. Biol. 1999; 214:102–112. [PubMed: 10491260]

Leptin M, Bogaert T, Lehmann R, Wilcox M. The Function of Ps Integrins During Drosophila Embryogenesis. Cell. 1989; 56:401–408. [PubMed: 2492451]

Ma X, Lynch HE, Scully PC, Hutson MS. Probing Embryonic Tissue Mechanics with Laser Hole-Drilling. Physical Biology. 2009; 6:036004. [PubMed: 19411738]

Markovsky I, Mahmoodi S. Least-Squares Contour Alignment. Signal Processing Letters, IEEE. 2009; 16:41–44.

Mashburn DN, Lynch HE, Ma X, Hutson MS. Enabling user-guided segmentation and tracking of surface-labeled cells in time-lapse image sets of living tissues. Cytometry. 2012; 81A:409–418. [PubMed: 22411907]

Means JC, Hays R. Mitochondrial membrane depolarization in *Drosophila* apoptosis. Cell Death Differ. 2007; 14:383–385. [PubMed: 16977330]

Oda H, Tsukita S. Real-time imaging of cell-cell adherens junctions reveals that Drosophila mesoderm invagination begins with two phases of apical constriction of cells. J. Cell Sci. 2001; 114:493–501. [PubMed: 11171319]

Peralta XG, Toyama Y, Tokutake Y, Hutson MS, Venakides S, Kiehart DP, Edwards GS. Upregulation of forces and morphogenic asymmetries in dorsal closure during *Drosophila* development. Biophys. J. 2007; 92:2583–2596. [PubMed: 17218455]

Rauzi M, Verant P, Lecuit T, Lenne PF. Nature and anisotropy of cortical forces orienting *Drosophila* tissue morphogenesis. Nature Cell Biology. 2008; 10:1401–1410.

Schöck F, Perrimon N. Cellular processes associated with germ band retraction in Drosophila. Dev. Biol. 2002; 248:29–39. [PubMed: 12142018]

Schöck F, Perrimon N. Retraction of the Drosophila germ band requires cell-matrix interaction. Genes Dev. 2003; 17:597–602. [PubMed: 12629042]

Sorrosal G, Pérez L, Herranz H, Milán M. Scarface, a secreted serine protease-like protein, regulates polarized localization of laminin A at the basement membrane of the Drosophila embryo. EMBO Rep. 2010; 11:373–379. [PubMed: 20379222]

Weisstein, EW. Area Moment of Inertia, pp. From Mathworld–A Wolfram Web Resourse. 2013. http://mathworld.wolfram.com/AreaMomentofInertia.html

Yip MLR, Lamka ML, Lipshitz HD. Control of germ-band retraction in Drosophila by the zinc-finger protein HINDSIGHT. Development. 1997; 124:2129–2141. [PubMed: 9187140]

Highlights (3 to 5 with maximum 85 characters per bullet point)

- In mid-GBR, segments in the crook of the germband are under anisotropic tension.
- Laser ablation of half the amnioserosa reduces this anisotropy.
- Laser ablation of half the amnioserosa causes failures in GBR.
- However, this failure is not identical to that of *ush* mutants.
- More localized ablation of specific amnioserosal regions phenocopies *mys* mutants.

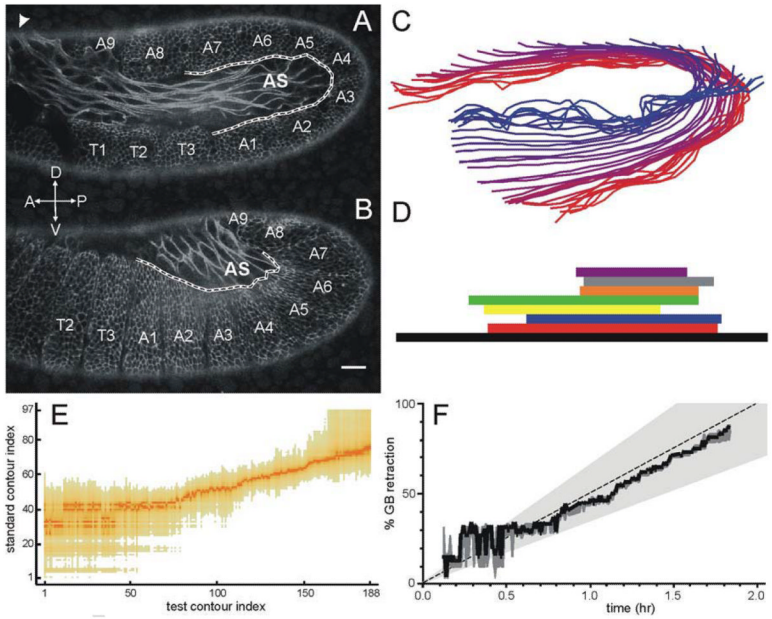

Figure 1.

Contour staging method. (**A**) Lateral view of an E-cadherin-GFP embryo in early germ band retraction showing a staging contour (*black dashed line surrounded by white*) that follows the amnioserosa-germband interface from segment boundary T3-A1 to A7-A8. The white arrows denote global anterioposterior (A-P) and dorsoventral (D-V) axes. The white arrowhead at top left denotes the thin bridge of cells that connects the two lateral flanks of amnioserosa. (**B**) Similar view and staging contour for an embryo in late germ band retraction. (**C**) Representative members of the standard set of contours. Colors shade from red to blue as the embryo progresses from early to late germ band retraction. (**D**) Temporal overlap between the eight time-lapse image sets used to construct the standard set. (**E**) Matrix of p-values for the alignment of each member of a “test” contour set against each member of the standard set. Darker colors correspond to more significant p-values and denote the best matches between sets. (**F**) Staging plot showing contour-based progression of the “test” set through germ band retraction: best fit (*solid line*); 95% confidence region (*dark gray shading*); and average progression rate of the standard set (*dashed line*) ± two standard deviations (*light gray shading*).

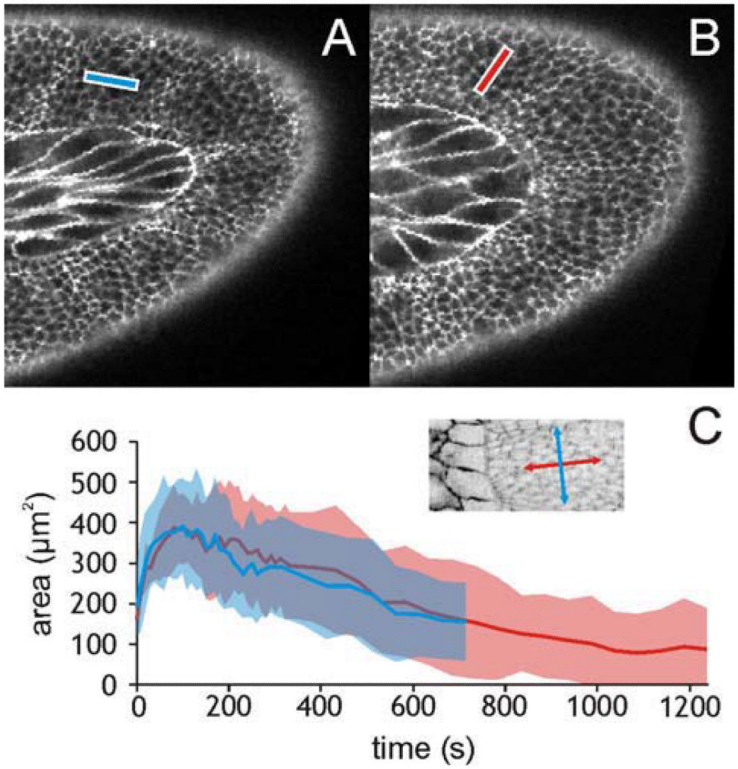

Figure 2.

Orientation of linear incisions in the germ band. (**A**) Targeted area for a 15-μm long laser incision along the *x*-axis of segment A5. (**B**) Same along the *y*-axis of A5. (**C**) Dynamics of wound area versus time for incisions along the *x*- (blue) and *y*- (red) axes of segment A7: mean (*solid lines*) ± one standard deviation (*shaded areas*). This graph is typical for both directions in all segments. The inset shows the orientation of segment-specific *x*- (*blue*) and *y*- (*red*) axes.

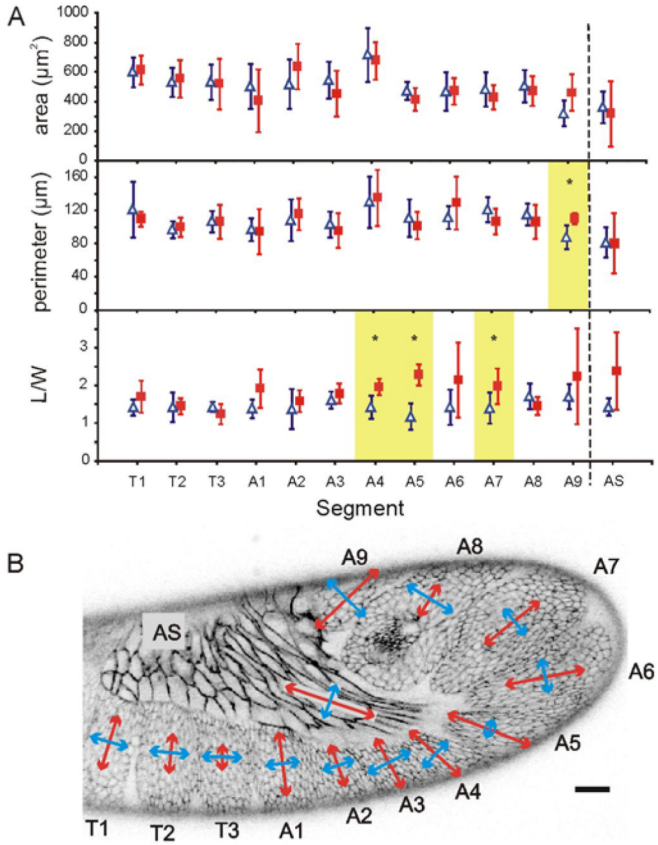

Figure 3.

Segment-dependence of wound expansion after 15-μm linear incisions. (**A**) Area (μm^2), perimeter (μm) and aspect ratio (L/W) of wounds at maximum expansion for incisions along the local segment-specific *x*- (*blue triangles*) or *y*- (*red squares*) axis. Error bars indicate ± one standard deviation. Significant differences ($p < 0.05$) in wound parameters for orthogonal incisions in a single segment are highlighted and marked with an asterisk. (**B**) Graphical representation of wound aspect ratios overlaid on an embryo at mid-germ band retraction. To emphasize regions with differences in aspect ratio the length of each double-headed arrow is L/W − 1. Arrows are aligned with the local segment-specific axes. Scale bar is 20 μm.

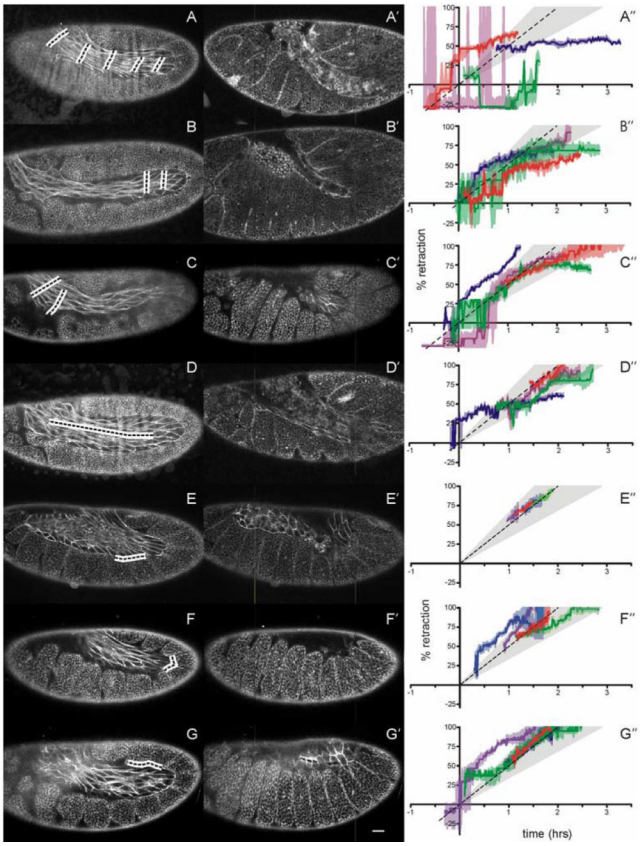

Figure 4.

Laser ablation of the amnioserosa during germ band retraction. (**A-G**) Confocal images of fly embryos before ablation of the marked regions (*blacked dashed lines surrounded by white*). (**A′-G′**) Same embryos after ablation. Images were taken at the time when germ band retraction would have completed in an unablated embryo. The common scale bar in G′ represents 20 μm. (**A″-G″**) Staging graphs corresponding to the ablation designs of A-G. Each colored curve represents retraction progress of a single experiment (shaded regions denote staging confidence intervals). The standard retraction rate (*dashed line*) ± two standard deviations (*light gray shading*) is shown for comparison. Curves similar in slope to the dashed line are retracting normally. Horizontal curves have stopped retracting.

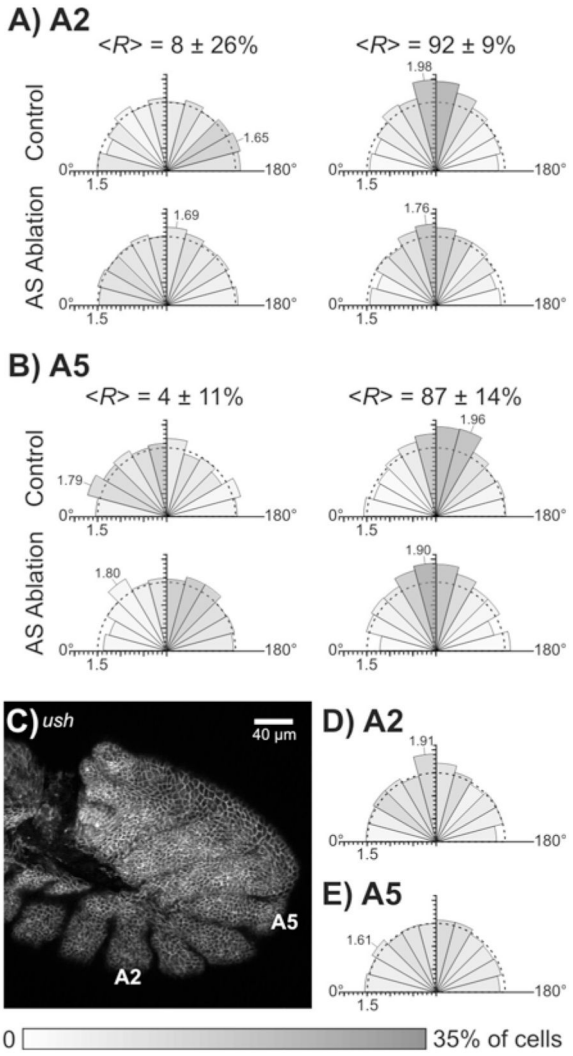

Figure 5.

Dynamic elongation and alignment of germ band cells in normal, laser-perturbed and *ush* mutant embryos. Each rose diagram compiles data from $N = 5$ embryos to detail cell shape and orientation. The shading of each sector represents the fraction of cells aligned in a particular direction – darker for larger fractions (grayscale bar at the bottom of the figure). The length of each wedge is proportional to the mean aspect ratio of cells aligned within that sector. An aspect ratio scale is provided by tick marks on the radial axis, a semicircle at a mean aspect ratio of 1.5, and labeling of sectors with the most elongated cells. An angle of 90° represents alignment of cells towards the amnioserosa, *i.e.*, along the local *y*-axis. **(A, B)** Dynamic cell shape changes tracked in segments A2 **(A)** and A5 **(B)** from early to late germ band retraction and in both control embryos and those in which one flank of the amnioserosa was ablated. The range of stages (R = % retraction) included in each control group is noted above each rose diagram as the mean ± one standard deviation. Control embryo images were stage-matched to the ablated embryo images based on pre-ablation stage and the elapsed time between pre- and post-ablation images (1-2 hours). A full set of individual rose diagrams for the ablated group is included as Supplemental Figure S1. **(C)** Confocal fluorescent image of a *ush/ush* embryo with anti-α-Spectrin staining. Scale bar is 40 μm. Although this embryo should have progressed to stage 13 or 14, it shows no evidence of any remaining amnioserosa cells and its germ band is unretracted. **(D, E)** Rose diagrams of cell

elongation and alignment in *ush/ush* embryos that failed to complete germ band retraction. There is very weak alignment of cells in segment A2 **(D)** towards where the amnioserosa would have been (near 90°) and essentially no extension or alignment of cells in segment A5 **(E)**.